Electrospun Biomimetic Fibrous Scaffold from Shape Memory Polymer of PDLLA-co-TMC for Bone Tissue Engineering

6 AUTHORS, INCLUDING:

Min Bao
Radboud University Nijmegen
8 PUBLICATIONS   **37** CITATIONS

SEE PROFILE

Qihui Zhou
University of Groningen
9 PUBLICATIONS   **46** CITATIONS

SEE PROFILE

Huihua Yuan
University of Wisconsin–Madison
19 PUBLICATIONS   **99** CITATIONS

SEE PROFILE

Yanzhong Zhang
Donghua University
73 PUBLICATIONS   **7,158** CITATIONS

SEE PROFILE

Electrospun Biomimetic Fibrous Scaffold from Shape Memory Polymer of PDLLA-*co*-TMC for Bone Tissue Engineering

Min Bao,[†,‡] Xiangxin Lou,[†,‡] Qihui Zhou,[†,‡] Wen Dong,[†,‡] Huihua Yuan,[†,‡] and Yanzhong Zhang*[,†,‡]

[†]State Key Laboratory for Modification of Chemical Fibers and Polymer Materials, Donghua University, Shanghai 201620, China
[‡]College of Chemistry, Chemical Engineering and Biotechnology, Donghua University, Shanghai 201620, China

S *Supporting Information*

ABSTRACT: Multifunctional fibrous scaffolds, which combine the capabilities of biomimicry to the native tissue architecture and shape memory effect (SME), are highly promising for the realization of functional tissue-engineered products with minimally invasive surgical implantation possibility. In this study, fibrous scaffolds of biodegradable poly(D,L-lactide-*co*-trimethylene carbonate) (denoted as PDLLA-*co*-TMC, or PLMC) with shape memory properties were fabricated by electrospinning. Morphology, thermal and mechanical properties as well as SME of the resultant fibrous structure were characterized using different techniques. And rat calvarial osteoblasts were cultured on the fibrous PLMC scaffolds to assess their suitability for bone tissue engineering. It is found that by varying the monomer ratio of DLLA:TMC from 5:5 to 9:1, fineness of the resultant PLMC fibers was attenuated from ca. 1500 down to 680 nm. This also allowed for readily modulating the glass transition temperature Tg (i.e., the switching temperature for actuating shape recovery) of the fibrous PLMC to fall between 19.2 and 44.2 °C, a temperature range relevant for biomedical applications in the human body. The PLMC fibers exhibited excellent shape memory properties with shape recovery ratios of $R_r > 94\%$ and shape fixity ratios of $R_f > 98\%$, and macroscopically demonstrated a fast shape recovery (~10 s at 39 °C) in the pre-deformed configurations. Biological assay results corroborated that the fibrous PLMC scaffolds were cytocompatible by supporting osteoblast adhesion and proliferation, and functionally promoted biomineralization-relevant alkaline phosphatase expression and mineral deposition. We envision the wide applicability of using the SME-capable biomimetic scaffolds for achieving enhanced efficacy in repairing various bone defects (e.g., as implants for healing bone screw holes or as barrier membranes for guided bone regeneration).

KEYWORDS: *Shape memory polymer, electrospun fibrous scaffold, bone tissue engineering, biomineralization, osteoblasts, poly(D,L-lactide-co-trimethylene carbonate)*
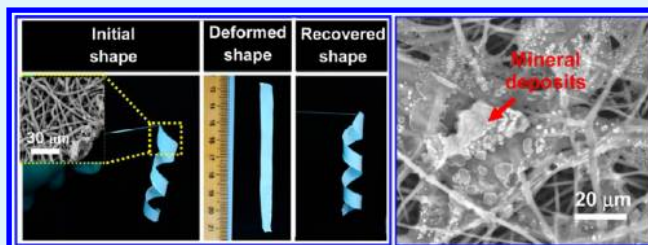
1. INTRODUCTION

Shape memory polymers (SMPs),[1] a class of stimuli-responsive smart materials, are of tremendous potential for application in medical implants that need to be delivered through minimal invasive surgery. This is owing to their intrinsic shape recovery capability,[2,3] which enables a bulky device packed in a small-sized temporary shape to go through narrow passages for deployment in the body, and then return to its original shape upon being actuated by a stimulus or trigger (e.g., temperature,[4] moisture,[5] magnetism,[6] and ultrasound[7,8]). In the past decade, while several SMP-based medical devices (or prototypes) have been explored for application in conventional biomedical engineering scenarios, such as cardiovascular stents,[4,9] self-tightening sutures,[10] dialysis needle adapters,[11] cold hibernated elastic memory foams for treating aneurysms[12] and thrombectomy device for clot removal,[13] shape memory properties have also gained interest in the field of tissue engineering and regenerative medicine (TERM) as an emerging strategy for creating intelligent tissue-engineered scaffolds/products to promote regeneration of functional tissues and organs *in vivo*.[14,15] In the context of SMPs for TERM, apart from their

basic capability of permitting minimally invasive surgical implantation for structural support, a biodegradable SMP for a particular tissue scaffolding can also be designed to allow for exerting appropriate stresses between the scaffolding constructs and surrounding tissues (beneficial for mechanotransduction-mediated tissue remodeling), regulating cell behavior by changing substrate topography,[16] and eluting therapeutical agents in a precisely controllable manner.[17] Undoubtedly, such an SMP-enabled intelligent scaffold integrated with multiple functionalities is highly promising towards ultimately enhancing the tissue repair and regeneration efficacy in the physiological environment upon implantation.

Electrospinning has been widely recognized as one of the most attractive enabling nanotechnologies to produce nano-scaled fibers that are suitable for a multitude of biomedical applications.[18] In particular, the use of electrospun nanofibers to construct biomimetic scaffolds for engineering diversified

tissues has been well-documented as they closely mimic the nanofibrillar components (e.g., collagen) of the extracellular matrix (ECM), which naturally surrounds the cells of any biological tissue.[19,20] Such nanofiber-based scaffolds with high porosity and specific surface area and nanotopography make them ideal candidates for engineering ECM to promote the cells functioning naturally. However, although a broad spectrum of SMPs based on synthetic polymers (e.g., polyurethanes),[21−26] natural biopolymers such as lignin,[27] or blend/composite systems[28,29] have recently been electrospun into nanofibers, which were also demonstrated to be distinctively advantageous in attaining rapid and efficient restoration of the predesigned structures in response to external stimuli,[23,26] hitherto very little work has been published on the design and performance of nanofibrous scaffolds with shape memory effect (SME) for defect repair or tissue regeneration applications.[6,30] In line with this, it also appears critically important to perform biocompatibility tests and functionality evaluation *in vitro* and *in vivo* using cells in contact with the nanofibrous SMP-based scaffolds as well as to examine the potential impact of SME on cell behavior.[14]

Here we present a thermoresponsive and biomimetic tissue engineering scaffold prepared by electrospinning a shape memory copolymer of poly(D,L-lactide-co-trimethylene carbonate) (PDLLA-co-TMC). In comparison with poly(D,L-lactide), one of the most studied homopolymers with shape memory properties for biomedical application, PDLLA-co-TMC from copolymerization of the D,L-lactide (DLLA) monomer and the trimethylene carbonate (TMC) monomer, is advantageous in tuning the recovery temperature of the material to suit for shape memory applications in human body. And also, both mechanical and degradation properties can be regulated by varying the molar ratio of DLLA and TMC.[31−35] In the past years, these copoly(estercarbonates) with outstanding tensile strength and flexibility have been investigated for applications as heart constructs and nerve regeneration guides,[33] cartilage implants and wound dressings, sustained drug release carriers,[35] annulus fibrosus closure devices[36] and stent covers.[33] However, to the best of our knowledge, no study on using the SME-capable nanofibrous scaffold for bone tissue engineering has been reported so far. Given the noted advantages in electrospun fibers and SMPs, an integration of shape memory properties (e.g., PDLLA-co-TMC and other different shape memory materials[37,38]) into nanofibrous structure is expected to achieve enhanced efficacy in repairing bone defects.

This work was designed to perform a sequential investigation of the followings: (i) electrospinning of PDLLA-co-TMC into ultrafine fibers in micro-/nanosized diameters; (ii) characterization of the morphology, thermal and mechanical properties as well as the shape memory properties of the fibrous PDLLA-co-TMC scaffolds, and (iii) examination of bone formation ability by culturing osteoblasts with the electrospun fibrous PDLLA-co-TMC scaffolds *in vitro*, so as to assess cytocompatibility in supporting cell adhesion and proliferation as well as biomineralization relevant outcomes including alkaline phosphatase expression and mineral deposition.

2. MATERIALS AND METHODS

2.1. Materials. PDLLA-co-TMC copolymers with varied DLLA:TMC feed ratios of 90:10, 80:20, 70:30 and 50:50 denoted, respectively, as PLMC (9:1), PLMC (8:2), PLMC (7:3) and PLMC (5:5) were purchased from Daigang Biomaterials (Jinan, China). Table 1 presents the molecular characteristics of these copolymers. N,N-

Table 1. Composition and Inherent Viscosity (IV) of PLMC Copolymers

samples	feed ratio (DLLA:TMC)	molar ratio[a] (DLLA:TMC)	IV[b] (dL g^{-1})
PLMC (9:1)	90:10	85:15	0.79
PLMC (8:2)	80:20	82:18	0.81
PLMC (7:3)	70:30	69:31	0.80
PLMC (5:5)	50:50	50:50	0.80

[a]Calculated from ^{1}H NMR (Avance 400, Bruker). [b]Determined by ubbelohde viscometers using chloroform as the dissolving solvent.

dimethylformamide (DMF) and dichloromethane (DCM) were commercial products from the Changshu Yang-Park Chemicals (Changshu, China). These materials and chemicals were used as received without further purification.

2.2. Electrospinning of PLMC Fibers. PLMC solution at a concentration of 20% w/v was prepared at room temperature by dissolving the polymer in DCM:DMF = 70:30 (v/v) for 12 h. The solution viscosity was determined by a viscometer (Thermosel, Brookfield, USA). Electrospinning was then performed using a set of variables as follows: an applied voltage of 16−18 kV, solution dispensing rate of 1.5 mL/h, collecting distance of 20 cm, ambient conditions of 45−50% humidity at 25−28 °C. To prepare fibrous PLMC scaffolds for cell culture, cover glasses with a diameter of 14 mm were placed on the aluminum foil to deposit fibrous membranes (thickness: ∼0.15 mm) onto coverslips. After electrospinning, all the electrospun samples were dried in a vacuum oven for over 2 days to remove any potential residual solvents.

2.3. Characterization. The electrospun fibers of PLMC were sputter-coated with gold and visualized by scanning electron microscopy (SEM) (Hitachi TM-1000, Tokyo, Japan) operated at an accelerating voltage of 10 kV. Fiber diameters were measured using ImageJ 1.40G software. At least 100 filaments of each sample from different SEM images were analyzed. The pore size and porosity of the electrospun fibrous PLMC membranes were measured on the basis of the previously reported methods.[39,40]

Differential scanning calorimetry (DSC) was employed to measure the thermal properties of the electrospun fibers of PLMC on a TA Instruments (204 F1 Netzsch, Germany) differential scanning calorimeter. Nitrogen was used as a purge gas with a flow rate of 20 mL/min. During the first heating run, the samples were heated from 0 to 70 °C with a heating rate of 10 °C/min, maintained at this temperature for 2 min, and then cooled down to 0 °C with a cooling rate of 10 °C/min. The second heating run was subsequently operated to generate DSC curves. The glass transition temperature (Tg) taken at the midpoint of the stepwise specific heat increment was determined from the second heating run.

Tensile mechanical properties of the electrospun fibrous membranes of PLMC were determined using a tabletop uniaxial material testing machine (H5K−S, Hounsfield, United Kingdom) equipped with a 10 N load cell. Rectangular-shaped specimens (50 × 10 × 0.10−0.15 mm) were stretched at a constant cross-head speed of 10 mm/min.

2.4. Shape Memory Effect. Dynamic mechanical analysis (DMA) (TA Instruments Q800, USA) was carried out to assess the shape memory properties of the fibrous PLMC membranes.[6,41,42] Briefly, samples with a dimension of 20 × 8 × 0.07 mm were thermally equilibrated at the temperature slightly above the Tg of the sample for 3 min to obtain a beginning strain (ε_{begin}) before the data were recorded. Stress was then increased from 0 to 0.9 MPa at a stress rate of 0.05 MPa s^{-1} to obtain a deformed strain (ε_{deform}) and fixed at 0.9 MPa while temperature was cooled down to 0 °C at a cooling rate of 2 °C min^{-1}. The temperature was equilibrated at 0 °C for 1 min, and then stress was isothermally unloaded back to 0 MPa to obtain a fixed strain (ε_{fix}). Finally, free-strain recovery was measured as the temperature was increased to the temperature slightly above the Tg of the sample at a heating rate of 2 °C min^{-1} to obtain a recovery
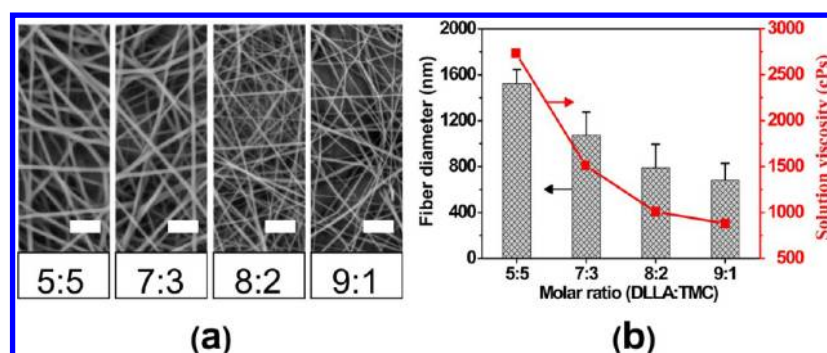
Figure 1. (a) SEM micrographs of electrospun fibers of PLMC with different DLLA:TMC molar ratios. Scale bars for the images represent 10 μm. (b) Effect of the TMC content on viscosity of the solutions and average diameter of the electrospun PLMC fibers.

strain (ε_{final}). The shape recovery ratio (R_r) and shape fixed ratio (R_f) were defined as follows:

$$R_r(\%) = \frac{\varepsilon_{deform} - \varepsilon_{final}}{\varepsilon_{deform} - \varepsilon_{begin}} \times 100\% \tag{1}$$

$$R_f(\%) = \frac{\varepsilon_{fix}}{\varepsilon_{deform}} \times 100\% \tag{2}$$

2.5. Biological Assays. *2.5.1. Isolation of the Primary Osteoblasts.* Calvarial fragments from newborn mice (Shanghai Laboratory Animal Center, Shanghai, China) were dissected and prepared as previously described.[43−45] In brief, the periosteum was removed and 1 mm² sized bone pieces were explanted into a 60 mm plate with PBS (Corning, CA, USA). For adherent culture, fragments were attached in the bottom of a 6-well tissue culture dish (Corning) containing 2 mL of low glucose Dulbecco's Modified Eagle's medium (DMEM) (Gibco, CA, USA) supplemented with 10% (v/v) fetal bovine serum (FBS, Gibco), 2 mmol/L glutamine (Gibco), 50 I.U./mL penicillin (Gibco), and 50 μg/mL streptomycin (Gibco). Cultures were maintained in a humidified atmosphere containing 5% CO_2 at 37 °C with medium changing twice a week. After 7 days of culture, outgrowth of osteoblast cells were harvested and trypsinized as primary osteoblast cells for uses in all biological experiments.

2.5.2. MTT Assay. The osteoblasts were seeded on the fibrous PLMC scaffolds and coverslips (as control) at a density of 5×10^4 cells per well in 24-well plates. Prior to cell seeding, all fibrous scaffolds were placed in a 24-well tissue culture plate (TCP) (JET-BIOFIL) and fixed with stainless steel rings, sterilized with ethanol for 2 h, and then soaked with medium overnight. Cell proliferation was monitored by MTT assay at the predetermined culturing time points of 1, 4 and 7 days. Briefly, the cells were washed with PBS and a 3-[4,5-dimethylthiazol-2-yl]-2,5-diphenyltetrazolium bromide (MTT) solution; 40 μL (5 mg/mL) was added to each well, followed by incubation for another 4 h. Then, 400 μL of DMSO (Sigma) was added to each well to dissolve the purple MTT formazan crystal for 15 min on an oscillator and 100 μL of the dissolved formazan solution of each sample was transferred into separate wells of a 96-well plate to test the optical density (OD) value at 570 nm using a microplate reader (MK3, Thermo, USA). Mean and standard deviation from the triplicate wells for each sample were reported. As a complementary test, the area of cell attachment was quantitatively measured by NIS-Elements imaging software for three randomly selected fields.

2.5.3. Cell Morphology Observation. To observe the cell morphology, cell-scaffold constructs were washed with PBS to remove the nonadherent cells and fixed with 4% paraformaldehyde for 3 h at room temperature. The constructs were further dehydrated through a series of graded alcohol solutions and finally dried overnight. After coating with gold, the dried cellular constructs were observed by SEM (Hitachi TM-1000, Tokyo, Japan) at an accelerating voltage of 10 kV.

Fluorescence staining was performed to assess the cytoskeletal organization of osteoblasts after 4 and 7 days of culture. Briefly, the harvested cell-scaffold constructs were fixed with 4.0% paraformaldehyde followed by washing for three times in PBS, and permeabilized

with 1 mL of 0.1% (v/v) Triton X-100 followed by washing for three times in PBS. Thereafter, the constructs were incubated with 150 μL of rhodamine−phalloidin (1:40 dilution in PBS, Sigma) for 30 min at room temperature in the dark followed by washing and incubating with 0.8 mg/mL 4′,6-diamidino-2-phenylindole (DAPI) (Sigma) in PBS for 15 min at 37 °C. The samples were then visualized with a fluorescent microscope (Nikon Eclipse TE 2000-U, AVON, MA).

2.5.4. Biomineralization Assays. Osteoblasts were seeded onto PLMC scaffolds and coverslips (as a control) at a density of 5×10^4 cells/well in 24-well plates (Corning, NY, USA) with 1 mL of DMEM/F12 medium (1:1) (Gibco, CA, USA) containing 10% FBS, 2 mmol/L glutamine (Gibco), 50 I.U./mL penicillin (Gibco), and 50 μg/mL streptomycin (Gibco). The medium was replaced every 3 days and incubated at 37 °C in a humidified atmosphere with 5% CO_2. Biomineralization assays including alkaline phosphatase (ALP) expression and mineral deposition were performed after 4 and 7 days of culture.

ALP activity was assayed using a BCIP/NBT alkaline phosphatase color development kit (Nanjing Jiancheng Bioengineering Institute), according to the manufacturer's specification. Briefly, cell-scaffold constructs were washed three times with PBS and 50 mL of cold 10 mM Tris/HCl buffer (pH 7.4) containing 0.1% Triton X-100 added prior to incubation at 4 °C overnight. A 100 μL volume of ALP substrate solution (2 mM $MgCl_2$ and 16 mM p-nitrophenyl phosphate) was then mixed with each sample. After incubation at 37 °C for 30 min, the reaction was stopped by the addition of 50 mL of 0.2 M NaOH and the liberated p-nitrophenol was measured spectrophotometrically at 405 nm.

To determine mineral deposits, cell-scaffold constructs were washed with PBS to remove the nonadherent cells and fixed in 4% paraformaldehyde for 3 h at room temperature. The morphology and elemental composition of mineral deposits were investigated by using SEM (JSM-5600 LV, Japan) and an energy-dispersive X-ray spectroscopy (EDXS) probe (IE 300 X) attached to the scanning electron microscope. Instrument aperture and probe current were adjusted to give a dead time of 15−20%. Surfaces were analyzed for 5 min at 5−15 kV and a magnification of 2000× to provide a complete profile of the different elements present. To further confirm the composition and crystalline structure of mineral deposits, the cellularized scaffolds before and after 7 days of culture were cut into pieces and XRD analysis was performed with the D/max-2550 PC (Japan) diffractometer. The operating voltage and current were kept at 40 kV and 300 mA, respectively. The samples were examined between 0 and 70° (2θ) at scanning rate of 1° (2θ) per min.

2.6. Statistical Analysis. Data were expressed as mean ± standard deviation and checked by normality tests. Statistical analysis was performed using Origin software. All the data was analyzed using one way analysis of variance (ANOVA) with Tukey's test to determine differences between groups. A value of $p < 0.05$ was considered to be statistically significant.

3. RESULTS AND DISCUSSION

3.1. Characterization of the Electrospun PLMC Fibers.
Fibrous PLMC mats with microscale interstitial pores and random orientation of the ultrafine fibers were obtained via electrospinning, as revealed by SEM images shown in Figure 1a. Diameters of the electrospun fibers of PLMC with varied DLLA:TMC ratios of 5:5, 7:3, 8:2 and 9:1 were measured to be 1526 ± 120, 1073 ± 201, 790 ± 204 and 682 ± 146 nm, respectively (Figure 1b). Clearly, the less molar ratio of TMC in the PLMC copolymer, the smaller diameter of the PLMC nanofibers resulted. This is most likely related to the change of solution viscosity in electrospinning. As shown in Figure 1b, the solution viscosity decreases from 2735 to 879 cPs with reducing the content of TMC from 5:5 to 9:1. It was reported that the solution viscosity, dictated mainly by polymer molecular weight[46] and concentration,[47] is one of the most important parameters influencing the morphology of electrospun nanofibers.[48] Higher solution viscosity usually gives rise to the increase of fiber diameter. Interestingly, even though we used nearly the same molecular weight of PLMC copolymer and solution concentration, it is found that variation of copolymerization ratio of the chemical composition DLLA and TMC also significantly affected the diameter of the resultant electrospun fibers, revealing that compositional ratio in copolymers is another determining factor affecting the fineness of electrospun fibers. Quantitative measurements indicate that these fibrous PLMC membranes possess an interfiber distance (pore size) in the range of 12.4–19.7 μm and porosity 71.8–79.3% (Table S1).

Figure 2 shows the thermal properties of the fibrous PLMC, which were determined by the second DSC heating scan. All
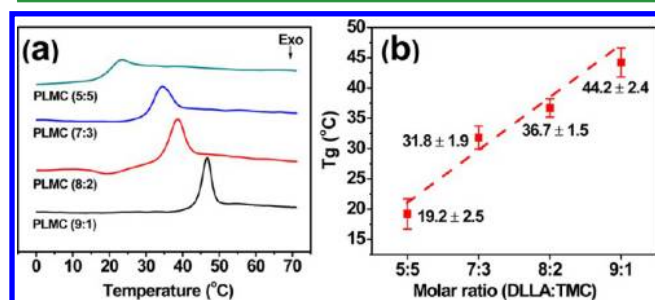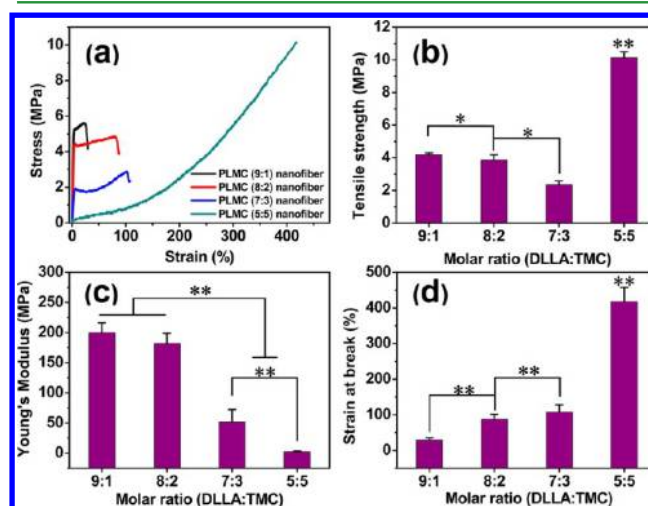

Figure 2. (a) DSC curves of the electrospun fibers of PLMC with varied DLLA:TMC ratios (5:5, 7:3, 8:2 and 9:1). These curves were recorded on the second heating run. (b) The derived Tg values of the electrospun PLMC fibers from panel a.

the copolymers of PLMC appear to be amorphous, as only the single glass transition is detected in their DSC curves. The Tg of PLMC (5:5) fibers is detected at 19.2 °C, indicating that it is a rubbery polymer at room temperature. Increasing the content of hard segment DLLA in PLMC (7:3, 8:2, and 9:1) resulted in sequential increase of Tg values of PLMC to 31.8, 36.7, and 44.2 °C, respectively. According to various application strategies, the transformation temperature T_{trans} of shape memory polymer may be suitably in different temperature ranges.[49] Consequently, a Tg, as the T_{trans} of PLMC in current study, between room temperature and body temperature may result in an automatically induced shape change after implantation. A Tg slightly above body temperature allows for on-demand control of the shape change (and synchronized with delivery of various biological agents, if any) by applying

heating either directly[14,16] or indirectly (e.g., ultrasound-irradiation,[7,8] magnetic field[6]). The present results demonstrated the feasibility of modulating the transformation temperature T_{trans} of the electrospun PLMC fibers by readily varying the ratio of DLLA:TMC upon constructing an implantable medical device for specific *in vivo* uses.

Mechanical performance is one of the essential requirements for a biomaterial to be used for a structure-supportive tissue scaffold. Figure 3 shows representative tensile stress–strain


Figure 3. Mechanical properties of the electrospun fibrous PLMC membranes (n > 6 for each type of PLMC) tested at room temperature. (a) Typical stress–strain curves, (b) tensile strength, (c) Young's modulus, and (d) strain at break. (*p < 0.05, **p < 0.01).

curves and derived tensile properties of the fibrous PLMC membranes with different DLLA:TMC compositions. It appears that the mechanical behavior of these fibers is markedly different, in particular governed by the DLLA:TMC ratio-correlated Tg values (Figure 2b). When the DLLA is dominant in PLMC, it gives rise to mechanical properties of materials in a stiff state. For instance, the specimen of PLMC (9:1) is characterized by a high Young's modulus (199.88 MPa) and a very low strain at break (< 30%). And PLMC (7:3) with a Tg slightly above room temperature also shows a higher Young's modulus of 52 MPa, although remarkably lower than that of the PLMC (9:1) fibers. In contrast, PLMC (5:5) fibers exhibit high tensile strength (10.16 MPa) and elongation (417.88%) as Tg of the PLMC (5:5) fibers is lower than room temperature, allowing for exhibiting rubbery behavior under the applied tensile testing conditions. Consequently, mechanical properties of the electrospun PLMC fibers varying from rigid and glassy state to flexible and rubber-like elastomer, can be readily tuned as well by varying the DLLA:TMC ratio. The mechanical properties are also comparable with other types of electrospun fibrous scaffolds for bone tissue engineering as reported in literature.[50−52]

3.2. SME of the Electrospun Fibrous PLMC Scaffolds.
It is known that the activation temperature T_{trans} of SMPs between room temperature and body temperature results in an automatically induced shape change after implantation, and T_{trans} slightly above the body temperature enables on-demand control of the shape recovery process by applying direct heating or thermal stimuli externally.[49] Therefore, we purposefully selected PLMC (8:2) (Tg = 36.7 °C) and PLMC (9:1) (Tg = 44.2 °C) fibers to investigate their shape memory effects by
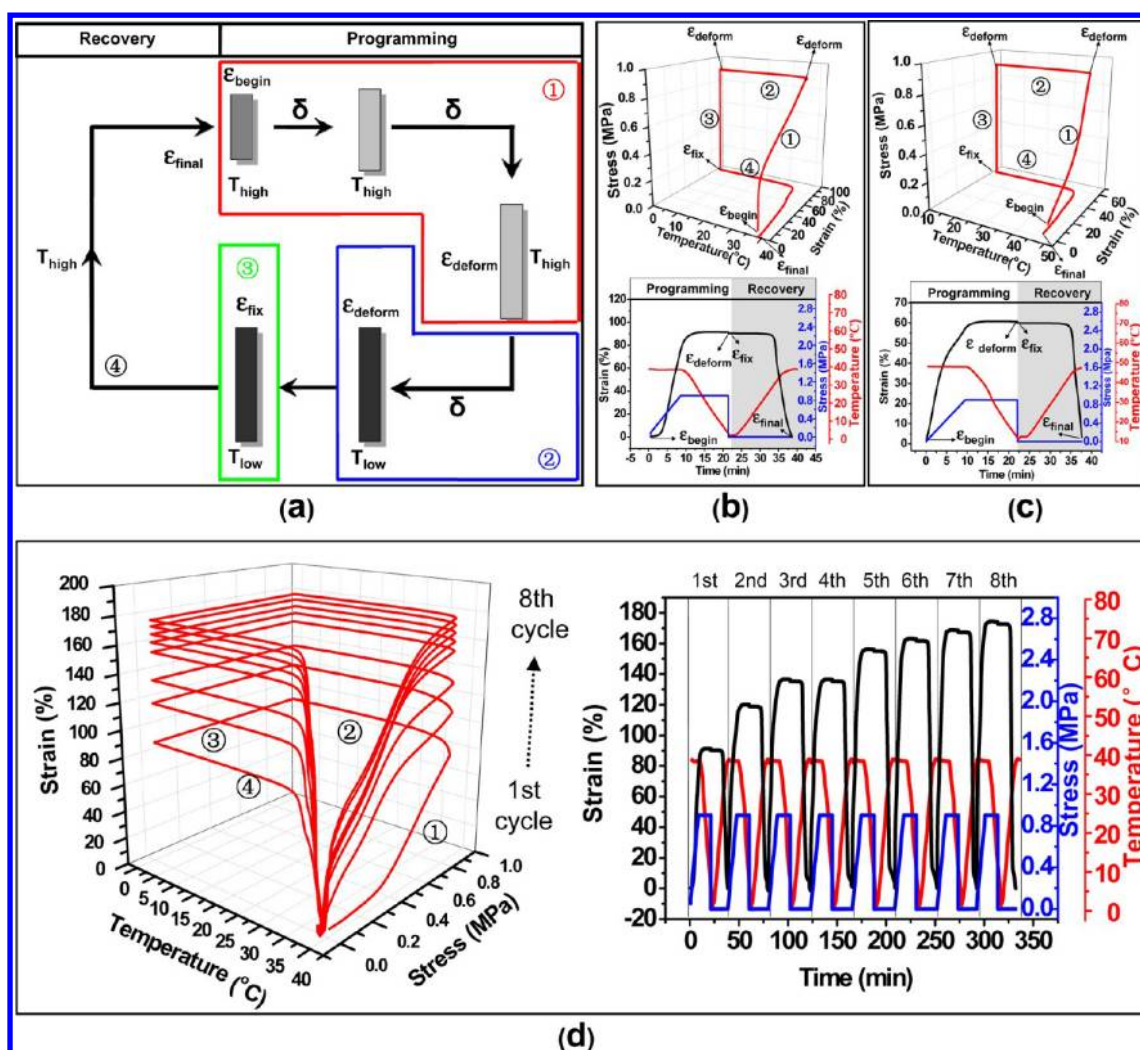
Figure 4. (a) Schematic representation of a cyclic shape memory test. (b, c) Three-dimensional shape memory stress−strain−temperature data, and two-dimensional illustration of strain, stress, and temperature versus time of (b) PLMC (8:2) and (c) PLMC (9:1) fibers. (d) Shape memory tests of PLMC (8:2) fibers repeated for eight times. Data plotted in (b, c, d) is from DMA testing.

DMA. A schematic representation of a cyclic shape memory test is illustrated in Figure 4a. Figure 4b,c shows the typical strain−stress−temperature curves of PLMC (8:2) and PLMC (9:1) nanofibers, respectively. Taking the PLMC (8:2) as an example to elaborate, the cyclic curve includes four steps (Figure 4b): (1) at 39 °C (slightly above the phase-transition temperature Tg (36.7 °C) of the PLMC (8:2) sample), PLMC was deformed as stress was increased from 0 to 0.9 MPa; (2) at the same stress level (i.e., 0.9 MPa) the temperature was decreased gradually to 0 °C for PLMC with the deformed shape; (3) at 0 °C the stress was removed; (4) the shape memory recovery was realized with the temperature increased to 39 °C.

Furthermore, a cyclic tensile test repeated up to eight times was carried out (Figure 4d). After the 8th cyclic shape memory test, the R_f and R_r of the electrospun PLMC (8:2) fibers were as high as 99.60% and 99.96%, respectively (Table 2). This demonstrated an excellent shape memory effect of the electrospun fibrous PLMC (8:2). The improved R_r values throughout the cyclic tests may be attributed to chain orientation after the previous cycle tests.[42] It is of note that with increases in the repeated times, the ε_{deform} becomes larger (from 91.39% at 1st cyclic to 173.38% at 8th cyclic), indicative of

Table 2. Some of the Measured SME Parameters of the Electrospun Nanofibrous PLMC (8:2) Repeated for Eight Cycles and PLMC (9:1) for One Cycle

sample	cycle	ε_{begin} (%)	ε_{deform} (%)	ε_{fix} (%)	ε_{final} (%)	R_f (%)	R_r (%)
PLMC (8:2)	1st	0.10	91.39	90.59	2.23	99.12	97.66
	2nd	2.23	120.51	119.86	3.09	99.46	99.27
	3rd	3.09	137.77	135.18	3.45	98.12	99.73
	4th	3.45	137.79	135.22	3.62	98.13	99.87
	5th	3.62	155.29	153.32	3.73	98.73	99.92
	6th	3.73	161.96	160.66	3.78	99.19	99.96
	7th	3.78	168.01	167.33	3.82	99.59	99.94
	8th	3.82	173.38	172.70	3.89	99.60	99.96
PLMC (9:1)	1st	0.03	60.88	59.76	3.68	98.16	94.00

a creep effect. Likewise, the electrospun fibrous PLMC (9:1) also demonstrated impressive shape memory effect although the shape recovery ratio (94.00%) of PLMC (9:1) in a cyclic thermomechanical experiment is slightly lower than that of PLMC (8:2) (97.66% at 1st cycle). This is because of higher content of the elastomeric TMC in PLMC (8:2), which may

2615

dx.doi.org/10.1021/am405101k | ACS Appl. Mater. Interfaces 2014, 6, 2611−2621
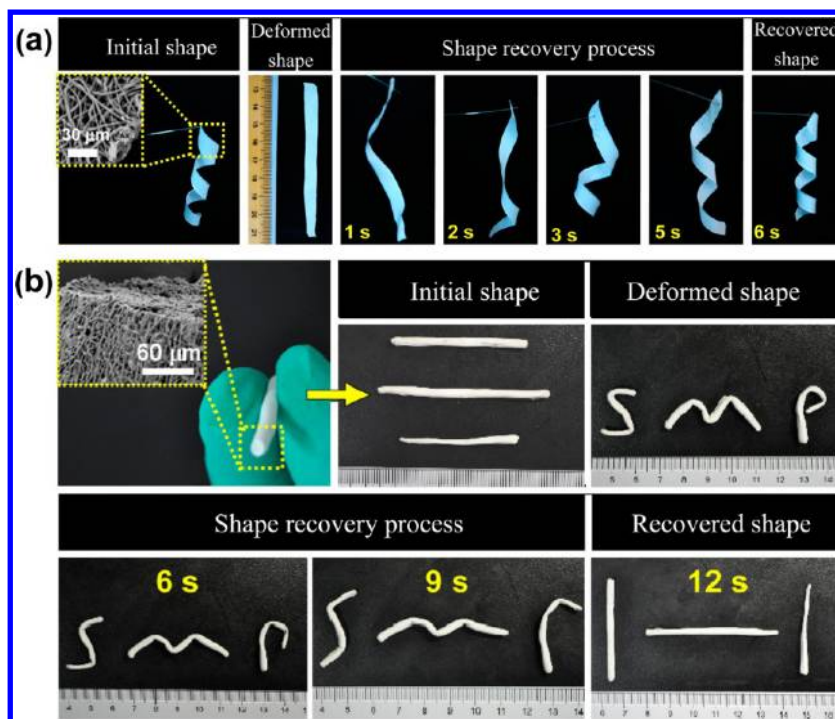
Figure 5. Macroscopic demonstration of the shape memory effect for electrospun fibrous PLMC (8:2). (a) Shape recovery process of a spiral in membranous form (2-D), obtained by rendering the sample strip wrapped around a rod (10 mm in diameter) in an oven at 39 °C for 20 s. Inset is an SEM image showing the fibrous morphology; (b) shape recovery process of the cylindrical bars made of electrospun fibers (inset image), in transition from the temporary shape ("SMP") to the permanent straight bars. In this experiment, these straight bars prepared by rolling-up of electrospun mats, were deformed at a temperature slightly above the Tg of PLMC (8:2) in a cylindrical mold (5 mm in diameter) for 30 s and then cooled to room temperature for fixing the deformed shapes. Shape recovery process was performed after re-immersion of the sample in the water bath at 39 °C. Pictures were taken by a digital camera after the samples were taken out from water bath at the predetermined time points.

contribute to enhanced driving force for shape recovery due to the entropy elasticity during phase transition.[53] A further examination on the fiber morphology after one cycle of shape deformation and recovery test indicates that the orientation of electrospun PLMC fibers (deformed state) could return to the initial random state (Figure S1, Supporting Information) after shape recovery process. And there is no significant change in mechanical properties except for a slight increase in the strain at break (Figure S2, Supporting Information).

Then, the fibrous PLMC (8:2) was again employed to demonstrate the macroscopic shape memory effect of fibrous structures in the forms of spiral and cylindrical bar, respectively. When the permanent (initial) shape of the membrane is a spiral (Figure 5a), the shape recovery from a temporary shape of straight strip can complete in a time scale of few seconds (~6 s) upon the deformed strip is dipped in the water bath at 39 °C, which is in the acceptable range of shape recovery temperature.[54−56] Likewise, a 3-D shaped structure also exhibited a good shape memory effect. As shown in Figure 5b, heat-triggered shape recovery processes of samples in the shapes of "S", "M", and "P" were all complete within 12 s. However, it took a little longer time to recover to their respective final shapes than the 2-D fibrous membrane. The microstructural variance between them is considered to be responsible for the difference. The 3-D shaped cylindrical bar had a densely packed and partially fused fibrous structure, which could have a detrimental effect on fibers in contact with the surrounding hot medium as the response rate is strongly governed by the transfer rate of the stimulus into the SMP. But current demonstrations, in accordance with previous reports,[26] generally indicate that SMPs made of electrospun ultrafine

fibers show a rapid shape recovery effect in a time frame of <1 min thanks to their high specific surface area. Thus, electrospun fibrous structure could be well-suited for situations requiring more immediate control of the activation or constructing devices where a particular triggering mechanism with a slow activation time (e.g., water uptake driving the SME)[5] is to be obviated.

Thermally activated SMPs display at least two phases, characterized by two distinct thermal transitions. The phase showing the higher transition temperature (associated with either a glass transition or a melting) acts as a physical cross-linker of the polymer chains and is responsible for the permanent shape. The second phase, with lower transition temperature, plays the role of a molecular switch. Then, when a stimulus is applied to facilitate molecular motion, shape recovery activation is induced and realized. Zini et al. reported that the linear PLLA-PGA-PTMC terpolymers exhibit shape memory behavior by chain entanglements.[57] It is also the case of PLMC copolymer.[58] The ability to deform the PLMC networks and to fix the deformed networks is determined by the mobility of the amorphous phase. The chains of PLMC networks go through a process from an oriented network in their deformed state to their random coil conformations when reheating to a temperature above Tg. This results in the macroscopic recovery of the original shape.[36]

As demonstrated in Figure 5, preparation of biodegradable nanofibers into either 2-D or 3-D structures from shape memory polymers enables such kind of biomimicking scaffolds to actively change their shape in a complex and predefined manner upon stimulation. With excellent shape changing tailorability, these biodegradable nanofibrous structures could
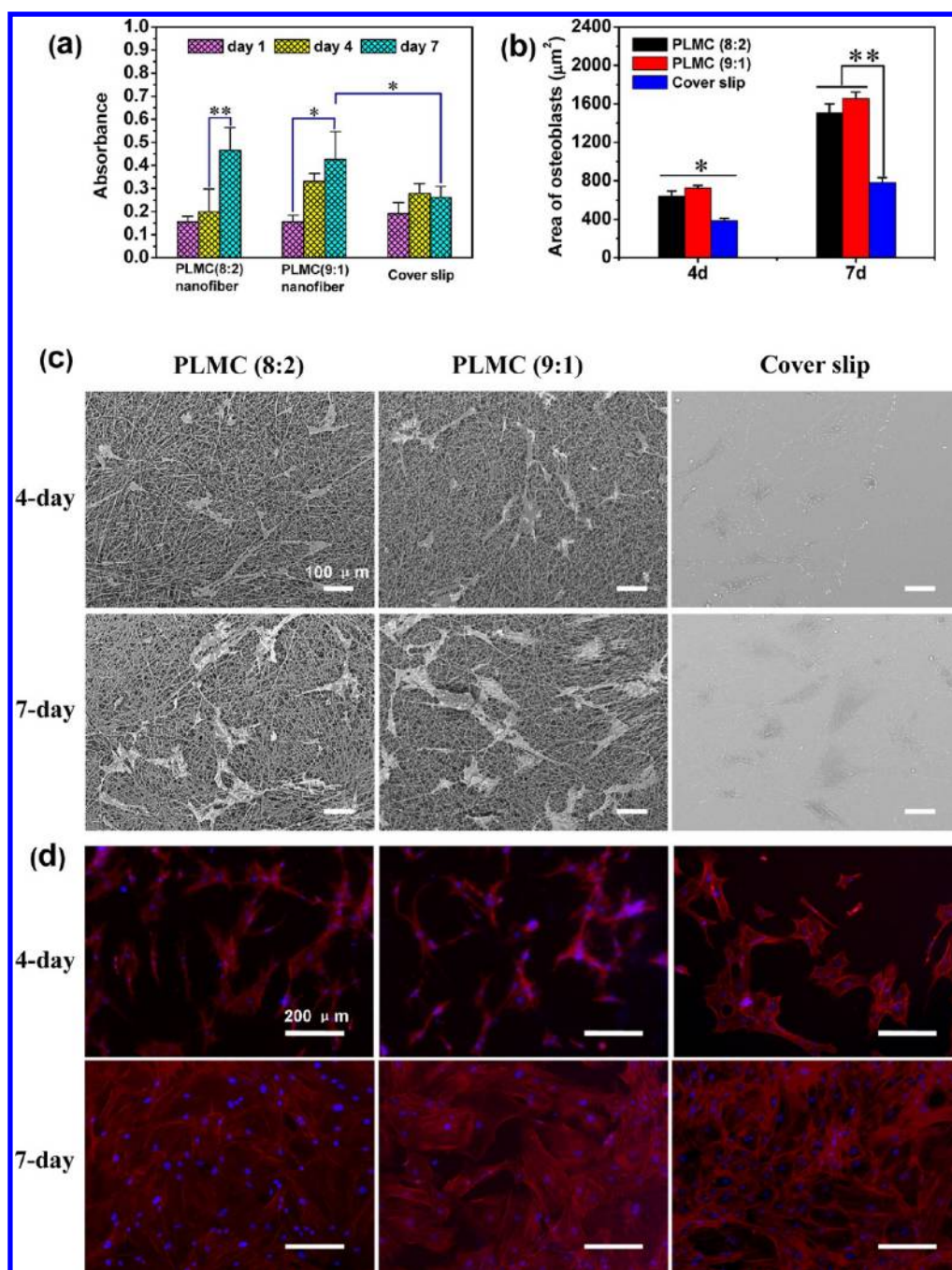
Figure 6. Proliferation and morphology observation of osteoblasts cultured onto the electrospun nanofibrous scaffolds of PLMC (8:2) and PLMC (9:1), and the coverslip control for up to 7 days. (a) Histogram of osteoblast proliferation by MTT assay; (b) histogram of area of osteoblasts; (c) SEM micrographs; (d) fluorescence staining of osteoblasts. F-actin filaments (red) and nucleus (blue) were stained by Phalloidin and DAPI, respectively. (*$p < 0.05$, compared to respective substrates at day 7, **$p < 0.01$).

be well-suited for use as self-deploying tissue-engineered scaffolds. For instances, although the 2-D nanofibrous membranes could be designed for constructing self-expandable vascular grafts,[9] the 3-D shaped cylindrical bar holds promise for utilization as resorbable screw-hole filler to reduce the likelihood of bone refracture after removal of repairing plates and screws.[59]

3.3. Bone Formation Ability. In bone tissue, it is the osteoblasts that are responsible for bone formation by secreting and mineralizing the bone matrix, which is composed mainly of type I collagen and the inorganic mineral hydroxyapatite (HAp). To test the efficacy of the nanofibrous PLMC scaffolds

on supporting osteoblast differentiation and bone formation, it is rational to examine the mineralization process of osteoblasts through *in vitro* culture, which is typically characterized by three stages, i.e., osteoblast proliferation, matrix maturation and matrix mineralization.[60]

3.3.1. Nanofibrous PLMC Scaffolds Promoted Osteoblast Proliferation. Cell adhesion, spreading and proliferation are important initial parameters in evaluating the cytocompatibility and suitability of a biomaterial for a specific application. A high degree of proliferation of cells is generally required as the proliferation degree determines the rate of extracellular matrix formation.
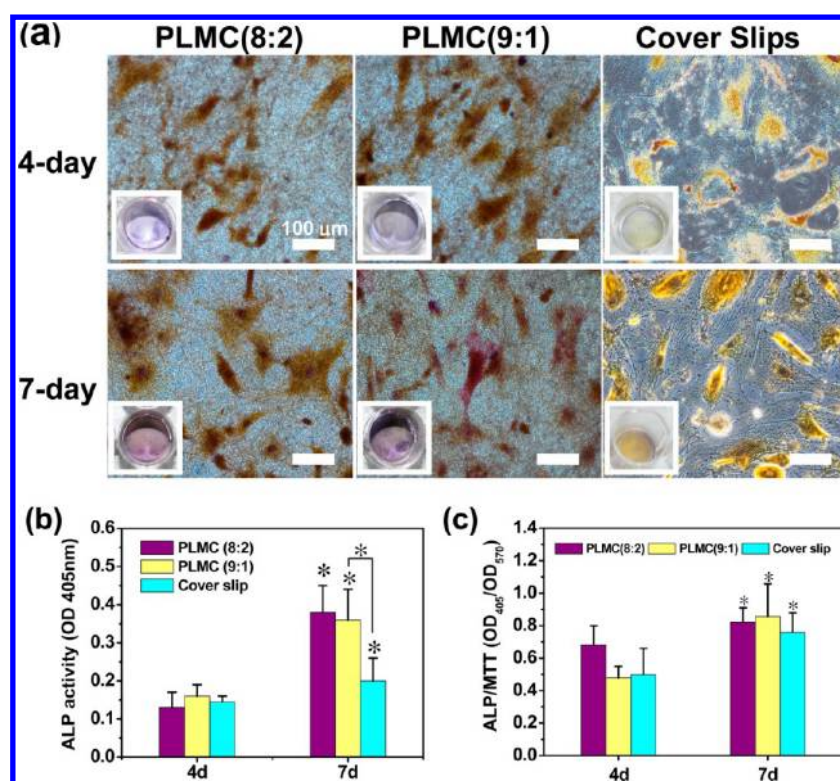
Figure 7. (a) ALP staining of osteoblasts attached onto electrospun fibrous PLMC (8:2, 9:1) and coverslips after 4 and 7 days of culture. Insets show macroscopic appearance. The stained cells via histochemical staining are in blue-violet color when ALP is present. (b) Quantitatively measured ALP activity, and (c) ALP activity normalized to osteoblast numbers. *$p < 0.05$ is from comparison to respective substrates at 4 days.

Nanofibrous scaffolds of PLMC (8:2) (Tg = 36.7 °C) and PLMC (9:1) (Tg = 44.2 °C) were selected to investigate their cytocompatibility. And in order to closely mimic the *in vivo* environment, osteoblasts isolated from newborn mice were utilized instead of a secondary-derived immortalized cell line (Figure S3, Supporting Information). The MTT assay data (Figure 6a) indicates that the attachment ability of osteoblasts cultured onto PLMC nanofibers and coverslips are comparable ($p > 0.05$) at day 1. At the time point of 7 days, the proliferation of cells cultured onto all nanofibrous scaffolds of PLMC (8:2 and 9:1) is significantly higher than that onto coverslips ($p < 0.05$). Interestingly, the proliferation of cells cultured onto PLMC (8:2) is slightly lower than other substrate at day 4. This subtle difference is likely associated with substrate stiffness.[61] Osteoblasts showed increased proliferation, motility and deposition of mineral on hard surfaces compared to soft substrates.[62] In addition, quantitative analysis of the area of cells (Figure 6b), which reflects the cellular spreading, adhesion and growth abilities demonstrated similar tendency as that of the cell proliferation results in Figure 6a. Of note, the cell area on both PLMC (8:2) and PLMC (9:1) scaffolds was nearly 2-fold larger than that on coverslips.

Morphology of osteoblasts attached and proliferated on the nanofibrous PLMC scaffolds was observed by scanning electron microscopy (Figure 6c). After 4 days of culture, there were more cells attached on nanofibrous scaffolds as compared to those grown on coverslips. After 7 days of culture, apart from increased cell numbers, there was an extensive network of cell lamellopodia and filopodia woven into and integrated well with the PLMC nanofibers, whereas the overall cell population was still noticeably less dense on coverslip than on nanofibrous scaffolds. These observations are in good agreement with the MTT and cell area data. To monitor the cell morphology of proliferating osteoblasts on the fibers, we also stained the cells after 4 and 7 days of culture (Figure 6d). Fluorescence images reveal an excellent adherence and spreading of the osteoblasts on the nanofibrous mats, in which the cells with well-shaped actin fibers and filopodia are visible. This is because actin-rich cell extensions are involved in cell adhesion, spreading, migration and intracellular communication.[63] Cells grown onto cover clips also display visible actin filaments on day 4, but their shapes become relatively thin and narrow on day 7. Moreover, an additional test at the cellular level examinations indicates that shape recovery process of the fibrous PLMC membranes did not exert an impact on cell viability (Figure S4, Supporting Information). Interestingly, SME of the fibrous PLMC scaffolds could be used to regulate cellular behavior (e.g., morphological change), which is in good accordance with a very recent report.[64]

Overall, the results shown in Figure 6 indicate that osteoblasts seeded on nanofibrous surfaces spread, migrate, adhere, and communicate much faster compared with that seeded on smooth surface of coverslips. This can be attributed to high specific surface area with these biomimetic nanofibers. Because osteoblasts are anchorage-dependent cells, the high specific surface area and porosity of electrospun fabrics could aid attachment and proliferation of cells on the scaffold. Our results thus demonstrated that the PLMC nanofibrous scaffolds have a good capability to prompt cell proliferation *in vitro*.

3.3.2. Nanofibrous PLMC Scaffolds Improved Total ALP Expression. ALP is a key component of bone matrix vesicles because of its role in mediating the formation of apatitic calcium phosphate on extracellular matrix proteins.[65] Proliferating osteoblasts show alkaline phosphatase activity, which is

greatly enhanced during *in vitro* bone formation. Elevated levels of ALP expression are typically observed several days prior to neo-mineralization and during the initial phase of bone matrix deposition. Therefore, ALP is a feasible marker for characterizing the matrix maturation stage. A successful bone scaffold must demonstrate support for enhanced ALP expression.

Results of the ALP staining of osteoblasts cultured on nanofibrous PLMC scaffolds and coverslips monitored after 4 and 7 days of cell seeding are shown in Figure 7a. There appears to be a positive influence of the nanofibrous PLMC scaffold on osteogenic differentiation. Osteoblasts cultured on the PLMC nanofibers exhibited significantly more ALP activity than those on the coverslips. Quantitative measurements of the ALP activity (Figure 7b) indicate that ALP produced by cells cultured on all substrates increased with increase in culture time from day 4 to day 7. The colorimetric ALP assay results at 4 days of culture showed no statistical difference between nanofibrous scaffolds and coverslips. However, the ALP activity of osteoblasts on PLMC nanofibers after 7 days of cell culture was 198% higher than that of those on coverslips. The result of ALP activities normalized to cell number according to previous study[66] is shown in Figure 7c. It can be seen that the osteogenic differentiation of osteoblasts grown on all the substrates used in this study is comparable and significantly enhanced when cultured up to 7 days ($p < 0.05$). Although substrate stiffness has been known to enhance the ALP expression,[61,67] the data suggests that these soft fibrous PLMC scaffolds still support higher amounts of total ALP expression, likely through enhancing the ability of cell proliferation. Taken together, these results demonstrate that the nanofibrous PLMC scaffolds possess a greater ability to support osteogenic differentiation.

3.3.3. Nanofibrous PLMC Scaffolds Supported Mineralization of Osteoblasts. Matrix mineralization stage involves a process that osteoblasts are induced to produce vast extracellular calcium deposits *in vitro*. Presence of calcium deposits is a remarkable indication of successful *in vitro* bone formation, in which the morphology and ultrastructure of the deposited minerals could be examined, respectively, by scanning electron microscopy, X-ray diffraction, and/or Alizarin Red S in bright orange-red.[62,68−71]

Figure 8a−d shows representative SEM images of the mineral deposition of osteoblasts on nanofibrous PLMC (8:2 and 9:1) scaffolds after 4 and 7 days of culture. The well-spread osteoblasts with good interaction with these nanofibrous scaffolds are clearly observed. Minerals in the form of globular accretions were deposited and aggregated on the basal surface of cells. Globular mineral deposits with the osteoblasts increased with increasing culture time from 4 to 7 days. These morphological observations are in good accordance with previous reports.[50,71]

The biologically mineralized constructs were also confirmed by performing the element analysis via EDXS imaging (Figure 8e). The amount of elemental Ca and P was measured from the surfaces of cells grown on nanofibrous scaffolds; it is known that Ca and P serve as the nucleating agent for HAp formation of bone. By EDXS, the Ca/P ratio of the mineral deposits on PLMC 9:1 and 8:2 was 1.76 ± 0.25 and 2.01 ± 0.07, respectively. Both these values are slightly higher than the stoichiometrical value of Ca/P in pure hydroxyapatite (1.67),[72] thus suggesting some degree of ionic substitution in the mineral formed in the cultures, such substitutions are also known to occur in bone.[73,74]
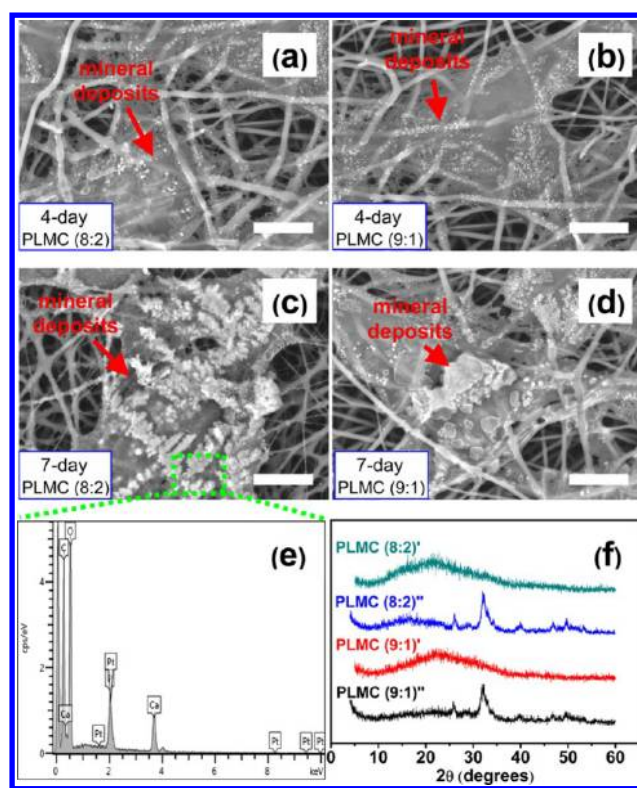
Figure 8. SEM micrographs of osteoblast interaction with PLMC (8:2) (a, c) and PLMC (9:1) (b, d) fibrous substrate after 4 and 7 days of culture. (Scale bars for the images are 20 μm.) (e) EDXS analysis for the detection of mineral deposits after culturing osteoblasts for 7 days with PLMC (8:2) fibers. (f) XRD patterns of fibrous scaffolds after 7 days of culturing with osteoblasts, where PLMC (8:2, 9:1) with the symbols of ' and " represent the scaffolds before and after cell culture, respectively.

To confirm the biophysical structure of the deposited minerals, XRD analysis on the cell−scaffold constructs was performed after 7 days of cell culture (Figure 8f). As HAp is the main inorganic component in natural bone, it is essential to corroborate the crystalline nature of the mineral deposits to be the same as that of the HAp. For the PLMC (8:2 and 9:1) nanofibrous scaffolds, before cell culture it shows a broadening hump at 2θ between 10° and 40°. After being cultivated with osteoblasts, presence of the characteristic (002) and (211) crystallographic planes, particularly at 26° and 32° of HAp, is observed. Results in Figure 8 thus solidly demonstrate the HAp nature of the deposited minerals. The formation of a mineralized matrix in a period of merely 7 days of osteoblast-scaffold cultivation is a significant result and indicates that the nanofibrous PLMC scaffolds, irrespective of the absence of the inorganic component of HAp, are still able to induce osteogenic differentiation and suitable for bone regeneration applications.[75]

This study reports on the electrospinning fabrication for the production of fibrous PLMC with shape memory effect and assesses the cellular responsive behavior pertaining to bone tissue engineering. A biomimetic and shape memory capable scaffold could ultimately enhance the bone regeneration efficacy upon transplantation. On the one hand, the overall topographical resemblance of electrospun nanofibrous scaffolds to the ECM architecture could provide a favorable milieu to naturally regulate cell adhesion, proliferation, differentiation and ECM production. On the other hand, an integration of

2619

dx.doi.org/10.1021/am405101k | *ACS Appl. Mater. Interfaces* 2014, 6, 2611−2621

SME functionality into the biomimetic scaffold would enable not only the possibility of implanting the scaffold in a compacted temporary shape through a small incision, but also offering biomechanics effect to allow for tissue remodeling upon activation of shape memory effect in a well-controlled manner. Our results here provide strong evidence that the SME-capable nanofibrous architecture of PLMC for osteoblasts scaffolding is beneficial for promoting bone formation relevant cell adhesion, proliferation, and mineralization *in vitro*. These preliminary results on cytocompatibility and bone formation ability warrant future work aimed at *in vivo* performance evaluation, encapsulation with therapeutic biomolecules and controllable shape recovery triggered by external stimulus such as high intensity focused ultrasound for the case of fibrous PLMC (9:1) with a relatively higher shape switching temperature or Tg.[7,8]

4. CONCLUSIONS

Preparation of biodegradable nanofibrous structures from SMPs can combine the biomimicking attribute of the nanofibers with the shape memory effects of the SMPs for minimally invasive surgical implantation and enhanced efficacy in tissue repair and regeneration. For the first time this study demonstrated that SME-capable nanofibrous PLMC copolymer can be successfully prepared via electrospinning. Varying compositional ratios of the building blocks DLLA and MTC in the PLMC copolymer allows for tuning of fiber fineness, Tg, and SMP mechanical properties over a wide range. Nanofibrous scaffolds of PLMC in 2-D and 3-D forms both exhibited excellent shape memory properties with impressive shape recovery ratios of $R_r > 94\%$ and shape fixity ratios of $R_f > 98\%$. The SME-capable nanofibrous scaffolds supported outstanding osteoblast attachement, proliferation and bone formation relevant outcomes such as ALP expression and hydroxyapatite-like mineral deposition. Taken together, current biomimetic nanofibrous PLMC scaffold integrated with desired functionalities including biodegradability, bone forming ability, and shape memory effect may be of great potential for achieving optimal outcomes in the course of scaffold-assisted bone repair and regeneration applications.

ASSOCIATED CONTENT

Ⓢ Supporting Information

Interfiber distance and porosity of fibrous PLMC mats (data are representatives of independent experiments and all data are given as mean ± SD), SEM images before and after shape recovery programming, plot of mechanical property of the electrospun PLMC fibers before and after shape recovery programming, description with images of isolation and identification of primary osteoblasts from calvarial fragments of newborn mice, images indicating the effect of shape recovery process on cell behavior and plot of the effect of shape recovery process on cell viability ($n = 4$). This material is available free of charge via the Internet at http://pubs.acs.org.

AUTHOR INFORMATION

Corresponding Author

*Yanzhong Zhang, Ph.D. Professor in Biomaterials, College of Chemistry, Chemical Engineering & Biotechnology, Donghua University, 2999 North Renmin Road, Shanghai 201620, China. Tel/Fax: +86 21 6779 2374. E-mail: yzzhang@dhu.edu.cn.

Notes

The authors declare no competing financial interest.

REFERENCES

(1) Lendlein, A.; Kelch, S. *Angew. Chem., Int. Ed.* **2002**, *41*, 2034−2057.
(2) Ratna, D.; Karger-Kocsis, J. *J. Mater. Sci.* **2008**, *43*, 254−269.
(3) Liu, C.; Qin, H.; Mather, P. *J. Mater. Chem.* **2007**, *17*, 1543−1558.
(4) Yakacki, C. M.; Shandas, R.; Lanning, C.; Rech, B.; Eckstein, A.; Gall, K. *Biomaterials* **2007**, *28*, 2255−2263.
(5) Huang, W.; Yang, B.; An, L.; Li, C.; Chan, Y. *Appl. Phys. Lett.* **2005**, *86*, 114105−114105-3.
(6) Gong, T.; Li, W.; Chen, H.; Wang, L.; Shao, S.; Zhou, S. *Acta Biomater.* **2012**, *8*, 1248−1259.
(7) Bao, M.; Zhou, Q.; Dong, W.; Lou, X.; Zhang, Y. *Biomacromolecules* **2013**, *14*, 1971−1979.
(8) Bao, M.; Tu, H.; Zhou, Q.; Dong, W.; Zhang, Y. *J. Controlled Release* **2013**, *172*, e110−e111.
(9) Venkatraman, S. S.; Tan, L. P.; Joso, J. F. D.; Boey, Y. C. F.; Wang, X. *Biomaterials* **2006**, *27*, 1573−1578.
(10) Lendlein, A.; Langer, R. *Science* **2002**, *296*, 1673−1676.
(11) Ortega, J. M.; Small, W.; Wilson, T. S.; Benett, W. J.; Loge, J. M.; Maitland, D. J. *IEEE Trans. Biomed. Eng.* **2007**, *54*, 1722−1724.
(12) Metcalfe, A.; Desfaits, A.-C.; Salazkin, I.; Yahia, L. H.; Sokolowski, W. M.; Raymond, J. *Biomaterials* **2003**, *24*, 491−497.
(13) Small, W., IV; Wilson, T.; Benett, W.; Loge, J.; Maitland, D. *Opt. Express* **2005**, *13*, 8204−8213.
(14) Neuss, S.; Blomenkamp, I.; Stainforth, R.; Boltersdorf, D.; Jansen, M.; Butz, N.; Perez-Bouza, A.; Knüchel, R. *Biomaterials* **2009**, *30*, 1697−1705.
(15) Thornton, A. J.; Alsberg, E.; Albertelli, M.; Mooney, D. J. *Transplant* **2004**, *77*, 1798−1803.
(16) Davis, K. A.; Burke, K. A.; Mather, P. T.; Henderson, J. H. *Biomaterials* **2011**, *32*, 2285−2293.
(17) Wischke, C.; Neffe, A. T.; Steuer, S.; Lendlein, A. *J. Controlled Release* **2009**, *138*, 243−250.
(18) Huang, Z.-M.; Zhang, Y.-Z.; Kotaki, M.; Ramakrishna, S. *Compos. Sci. Technol.* **2003**, *63*, 2223−2253.
(19) Sell, S.; Barnes, C.; Smith, M.; McClure, M.; Madurantakam, P.; Grant, J.; McManus, M.; Bowlin, G. *Polym. Int.* **2007**, *56*, 1349−1360.
(20) Pham, Q. P.; Sharma, U.; Mikos, A. G. *Tissue Eng.* **2006**, *12*, 1197−1211.
(21) Matsumoto, H.; Ishiguro, T.; Konosu, Y.; Minagawa, M.; Tanioka, A.; Richau, K.; Kratz, K.; Lendlein, A. *Eur. Polym. J.* **2012**, *48*, 1866−1874.
(22) Kratz, K.; Habermann, R.; Becker, T.; Richau, K.; Lendlein, A. *Int. J. Artif. Organs* **2011**, *34*, 225−230.
(23) Chen, H.; Cao, X.; Zhang, J.; Zhang, J.; Ma, Y.; Shi, G.; Ke, Y.; Tong, D.; Jiang, L. *J. Mater. Chem.* **2012**, *22*, 22387−22391.
(24) Zhuo, H.; Hu, J.; Chen, S. *J. Mater. Sci.* **2011**, *46*, 3464−3469.
(25) Lu, X.; Sun, Z.; Cai, W.; Gao, Z. *J. Mater. Sci.: Mater. Med.* **2008**, *19*, 395−399.
(26) Zhang, J.-N.; Ma, Y.-M.; Zhang, J.-J.; Xu, D.; Yang, Q.-L.; Guan, J.-G.; Cao, X.-Y.; Jiang, L. *Mater. Lett.* **2011**, *65*, 3639−3642.

(27) Dallmeyer, I.; Chowdhury, S.; Kadla, J. F. *Biomacromolecules* **2013**, *14*, 2354−2363.

(28) Luo, X.; Mather, P. T. *ACS Macro Lett.* **2013**, *2*, 152−156.

(29) Rodriguez, E. D.; Weed, D. C.; Mather, P. T. *Macromol. Chem. Phys.* **2013**, *214*, 1247−1257.

(30) Tseng, L.-F.; Mather, P. T.; Henderson, J. H. *Acta Biomater.* **2013**, *9*, 8790−8801.

(31) Andronova, N.; Albertsson, A.-C. *Biomacromolecules* **2006**, *7*, 1489−1495.

(32) Asplund, B.; Sperens, J.; Mathisen, T.; Hilborn, J. *J. Biomater. Sci., Polym. Ed.* **2006**, *17*, 615−630.

(33) Pego, A.; Van Luyn, M.; Brouwer, L.; Van Wachem, P.; Poot, A.; Grijpma, D.; Feijen, J. *J. Biomed. Mater. Res., Part A* **2003**, *67*, 1044−1054.

(34) Pêgo, A. P.; Poot, A. A.; Grijpma, D. W.; Feijen, J. *J. Controlled Release* **2003**, *87*, 69−79.

(35) Zhu, K.; Zhang, J.; Wang, C.; Yasuda, H.; Ichimaru, A.; Yamamoto, K. *J. Microencapsulation* **2003**, *20*, 731−743.

(36) Sharifi, S.; van Kooten, T. G.; Kranenburg, H.-J. C.; Meij, B. P.; Behl, M.; Lendlein, A.; Grijpma, D. W. *Biomaterials* **2013**, *34*, 8105−8113.

(37) Zhang, D.; Petersen, K. M.; Grunlan, M. A. *ACS Appl. Mater. Interfaces* **2012**, *5*, 186−191.

(38) Baker, R. M.; Henderson, J. H.; Mather, P. T. *J. Mater. Chem. B* **2013**, *1*, 4916−4920.

(39) Drexler, J.; Powell, H. *Acta Biomater.* **2011**, *7*, 1133−1139.

(40) Zheng, F.; Wang, S.; Wen, S.; Shen, M.; Zhu, M.; Shi, X. *Biomaterials* **2012**, *34*, 1402−1412.

(41) Guo, W.; Kang, H.; Chen, Y.; Guo, B.; Zhang, L. *ACS Appl. Mater. Interfaces* **2012**, *4*, 4006−4014.

(42) Guo, B.; Chen, Y.; Lei, Y.; Zhang, L.; Zhou, W. Y.; Rabie, A. B. M.; Zhao, J. *Biomacromolecules* **2011**, *12*, 1312−1321.

(43) Wiemann, M.; Gramsch, B.; Winterhager, E.; Schirrmacher, K. *Materialwiss. Werkstofftech.* **2004**, *35*, 962−967.

(44) Gerber, I.; Ap Gwynn, I. *Eur. Cells Mater.* **2001**, *2*, 10−20.

(45) Ecarot-Charrier, B.; Glorieux, F. H.; Van Der Rest, M.; Pereira, G. *J. Cell Biol.* **1983**, *96*, 639−643.

(46) Fukushima, S.; Karube, Y.; Kawakami, H. *Polym. J. (Tokyo, Jpn.)* **2010**, *42*, 514−518.

(47) Zhou, Q.; Bao, M.; Yuan, H.; Zhao, S.; Dong, W.; Zhang, Y. *Polymer* **2013**, *54*, 6867−6876.

(48) Deitzel, J.; Kleinmeyer, J.; Harris, D. e. a.; Beck Tan, N. *Polymer* **2001**, *42*, 261−272.

(49) Lendlein, A.; Zotzmann, J. r.; Feng, Y.; Alteheld, A.; Kelch, S. *Biomacromolecules* **2009**, *10*, 975−982.

(50) Prabhakaran, M. P.; Venugopal, J.; Ramakrishna, S. *Acta Biomater.* **2009**, *5*, 2884−2893.

(51) Fujihara, K.; Kotaki, M.; Ramakrishna, S. *Biomaterials* **2005**, *26*, 4139−4147.

(52) Zhang, Y. Z.; Reddy, V. J.; Wong, S. Y.; Li, X.; Su, B.; Ramakrishna, S.; Lim, C. T. *Tissue Eng., Part A* **2010**, *16*, 1949−1960.

(53) Xu, J.; Song, J. *Proc. Natl. Acad. Sci. U. S. A.* **2010**, *107*, 7652−7657.

(54) Guo, B. C.; Chen, Y. W.; Lei, Y. D.; Zhang, L. Q.; Zhou, W. Y.; Rabie, A. B. M.; Zhao, J. Q. *Biomacromolecules* **2011**, *12*, 1312−1321.

(55) Yakacki, C. M. *Polym. Rev.* **2013**, *53*, 1−5.

(56) Xue, L.; Dai, S. Y.; Li, Z. *Macromolecules* **2009**, *42*, 964−972.

(57) Zini, E.; Scandola, M.; Dobrzynski, P.; Kasperczyk, J.; Bero, M. *Biomacromolecules* **2007**, *8*, 3661−3667.

(58) Yang, J.; Liu, F.; Yang, L.; Li, S. *Eur. Polym. J.* **2010**, *46*, 783−791.

(59) Rosson, J.; Egan, J.; Shearer, J.; Monro, P. *J. Bone Jt. Surg., Br. Vol.* **1991**, *73*, 283−286.

(60) Stein, G. S.; Lian, J. B. *Endocr. Rev.* **1993**, *14*, 424−442.

(61) Grinnell, F.; Ho, C. H. *Biomaterials* **2013**, *34*, 965−974.

(62) Kharaziha, M.; Fathi, M.; Edris, H. *J. Mech. Behav. Biomed. Mater.* **2013**, *24*, 9−20.

(63) Rottner, K.; Behrendt, B.; Small, J. V.; Wehland, J. *Nat. Cell Biol.* **1999**, *1*, 321−322.

(64) Tseng, L.-F.; Mather, P. T.; Henderson, J. H. *Acta Biomater.* **2013**, *9*, 8790−8801.

(65) Anderson, H. C.; Sipe, J. B.; Hessle, L.; Dhamyamraju, R.; Atti, E.; Camacho, N. P.; Millán, J. L. *Am. J. Pathol.* **2004**, *164*, 841−847.

(66) Chen, J.-P.; Chen, S.-H.; Lai, G.-J. *Nanoscale Res. Lett.* **2012**, *7*, 1−11.

(67) Chatterjee, K.; Lin-Gibson, S.; Wallace, W. E.; Parekh, S. H.; Lee, Y. J.; Cicerone, M. T.; Young, M. F.; Simon, C. G., Jr *Biomaterials* **2010**, *31*, 5051−5062.

(68) Ravichandran, R.; Venugopal, J. R.; Sundarrajan, S.; Mukherjee, S.; Ramakrishna, S. *Biomaterials* **2012**, *33*, 846−855.

(69) Zhang, Y.; Venugopal, J. R.; El-Turki, A.; Ramakrishna, S.; Su, B.; Lim, C. T. *Biomaterials* **2008**, *29*, 4314−4322.

(70) Ravichandran, R.; Ng, C. C.; Liao, S.; Pliszka, D.; Raghunath, M.; Ramakrishna, S.; Chan, C. K. *Biomed. Mater.* **2012**, *7*, 015001.

(71) Zhang, Y.; Reddy, V. J.; Wong, S. Y.; Li, X.; Su, B.; Ramakrishna, S.; Lim, C. T. *Tissue Eng., Part A* **2010**, *16*, 1949−1960.

(72) Lee, R. S.; Kayser, M. V.; Ali, S. Y. *J. Anat.* **2006**, *208*, 13−19.

(73) Nakano, Y.; Addison, W. N.; Kaartinen, M. T. *Bone* **2007**, *41*, 549−561.

(74) Rey, C.; Beshah, K.; Griffin, R.; Glimcher, M. *J. Bone Miner. Res.* **1991**, *6*, 515−525.

(75) Yoshimoto, H.; Shin, Y.; Terai, H.; Vacanti, J. *Biomaterials* **2003**, *24*, 2077−2082.